Rock Mech. Rock Engng. (2006) 39 (3), 215–232
DOI 10.1007/s00603-005-0076-1

Rock Mechanics and Rock Engineering
Printed in Austria

Stress–Strain Model for Carbonate Rocks Based on Haldane's Distribution Function

By

V. Palchik

Department of Geological and Environmental Sciences,
Ben-Gurion University of the Negev, Beer-Sheva, Israel

Received May 7, 2004; accepted August 4, 2005
Published online November 21, 2005

Summary

This paper presents a model created by the author to predict stress–strain relationships for weak to strong carbonate rocks ($\sigma_c < 100$ MPa) exhibiting axial strains up to 1%. The stress–strain model based on Haldane's distribution function (Haldane, 1919) relates the axial stress (or normalized axial stress) to the square of an exponential function where the exponent is axial strain. To obtain accurate stress–strain relationship over the whole pre-failure strain with the proposed stress–strain model, it is necessary to have only one datum point (peak axial stress and maximum axial strain at this peak stress). It is shown that the stress–strain relationships observed in laboratory compression tests on samples collected from six carbonate rock formations (chalk, dolomites and limestones) from different parts of Israel, agree well with the stress–strain prediction model proposed by the author.

Keywords: Haldane's function, stress–strain model, uniaxial compressive stress.

1. Introduction

The stress–strain relationships for soils and rocks have been studied by many researchers (e.g. Kodner, 1963; Duncan and Chang, 1970; Haas, 1989; Tatsuoka and Shibuya, 1992; Tharp and Scarbrough, 1994; Muravskii, 1996; Puzrin and Burland, 1996; Ching et al., 1997; Fairhurst and Hudson, 1999; Gutierrez et al., 2000; Shibuya, 2002; Chang et al., 2002; Habimana et al., 2002). Hyperbolic (Kodner, 1963; Duncan and Chang, 1970; Tharp and Scarbrough, 1994; Habimana et al., 2002), logarithmic (Puzrin and Burland, 1996) and double exponential (Shibuya, 2002) stress–strain models for different rock types were proposed.

Some recent models (e.g. Tatsuoka and Shibuya, 1992; Puzrin and Burland, 1996; Shibuya, 2002) can provide a better approximation of stress–strain data over the whole pre-failure strain range. However, three free constants are involved in the double exponential fitting of the stress–strain model proposed by Shibuya (2002) and, therefore, three

data points over the pre-failure strain range are always required for successful fitting. The model relates the normalized stress to the normalized tangent Young's modulus:

$$\frac{\sigma_a}{\sigma_c} = \left[1 - \left(\frac{E_{\tan}}{AE_{\max}}\right)^{\frac{1}{k}}\right]^{\frac{1}{m}}, \tag{1}$$

where A, k and m are three free constants, for the determination of which three data points are necessary; σ_a is axial stress, σ_c is uniaxial compressive strength, E_{tan}/E_{max}

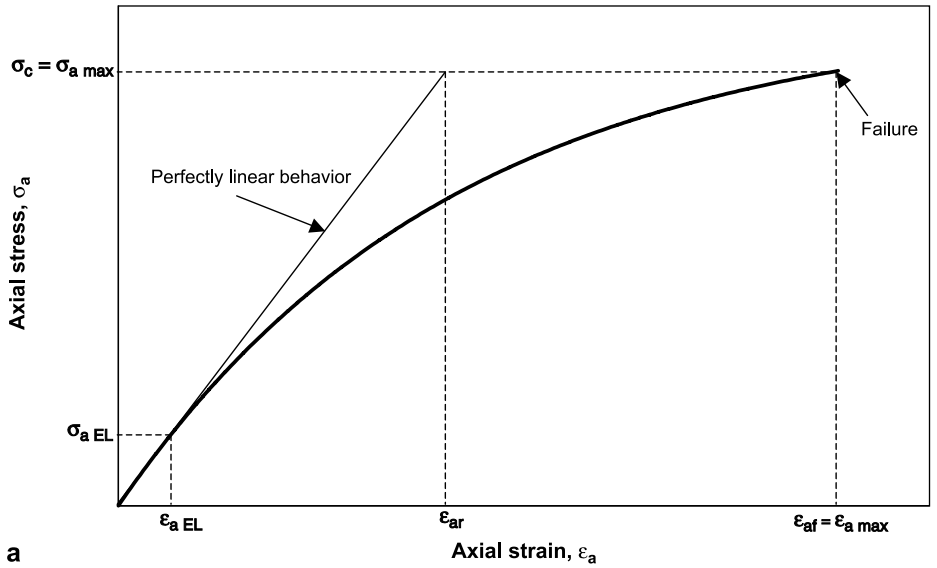

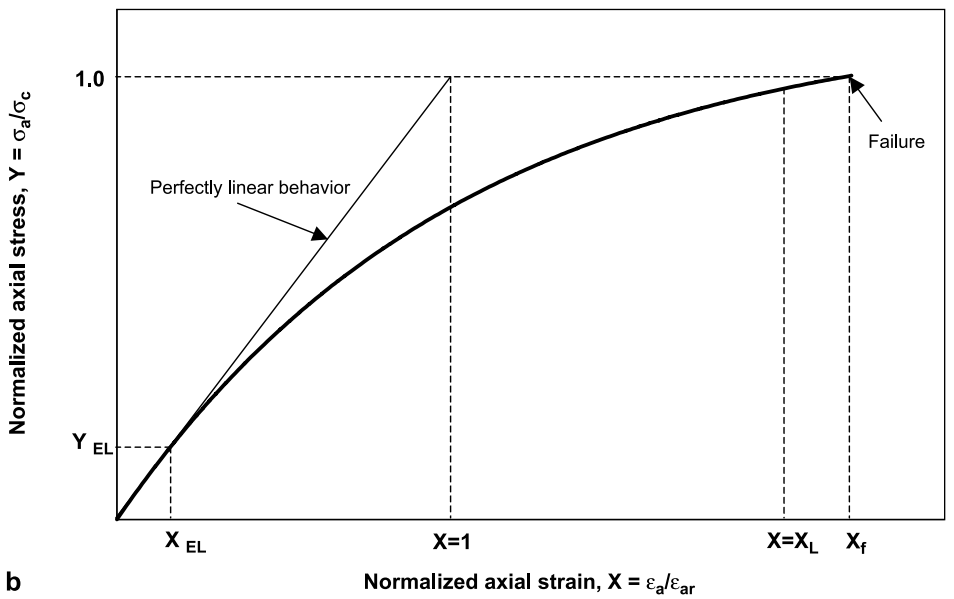

Fig. 1. Actual stress–strain curve (**a**) and normalized stress–strain curve (**b**) (after Shibuya, 2002). $\sigma_c = \sigma_{a\ max}$, $\varepsilon_{ar} = (\sigma_c/\sigma_{a\ EL})\ \varepsilon_{a\ EL}$ and $\varepsilon_{af} = \varepsilon_{a\ max}$

is normalized tangent Young's modulus, $E_{max} = \sigma_c/\varepsilon_{ar}$ and $\varepsilon_{ar} = (\sigma_c/\sigma_{a\,EL})\varepsilon_{a\,EL}$ (see Fig. 1) where $\sigma_{a\,EL}$ is axial stress at the elastic-threshold axial strain ($\varepsilon_{a\,EL}$, Fig. 1).

The actual stress–strain curve and the normalized stress–strain curve are shown in Fig. 1. Here, σ_c is maximum value of σ_a, and the maximum value of ε_a is the axial strain at the failure (ε_{af}).

A modified form of the hyperbolic model proposed by Tatsuoka and Shibuya (1992) also has a large number of involved parameters, which increases the number of data points needed for representing the stress–strain curve. The model has the following mathematical form:

$$\frac{\sigma_a}{\sigma_c} = Y_{EL} + \frac{\frac{\varepsilon_a}{\varepsilon_{ar}} - X_{EL}}{\frac{1}{C_1} + \frac{\frac{\varepsilon_a}{\varepsilon_{ar}} - X_{EL}}{C_2}}, \tag{2}$$

where σ_a/σ_c is the normalized axial stress, $\varepsilon_a/\varepsilon_{ar}$ is the normalized axial strain, Y_{EL} is normalized stress at the elastic-threshold axial strain (see Fig. 1), X_{EL} is the normalized elastic-threshold axial strain (see Fig. 1), C_1 and C_2 are coefficients which vary with the current strain level.

The logarithmic stress–strain model proposed by Puzrin and Burland (1996) has the following mathematical form when small strain data are not available:

$$\frac{\sigma_a}{\sigma_c} = \frac{\varepsilon_a}{\varepsilon_{ar}} - \alpha\frac{\varepsilon_a}{\varepsilon_{ar}}\left[\ln\left(1 + \frac{\varepsilon_a}{\varepsilon_{ar}}\right)\right]^R, \tag{3}$$

where α and R are two constants, σ_a/σ_c is the normalized axial stress and $\varepsilon_a/\varepsilon_{ar}$ is the normalized axial strain.

The model requires the values of normalized axial strain at two points (limiting strain and strain at the peak stress) to calculate the constants α and R. The point $X = X_L$ in Fig. 1b indicates the normalized limiting strain.

Note that the stress–strain models mentioned above can be used only for rocks which exhibit small to intermediate axial strain (ε_a less than 0.5%).

In this paper, the author proposes a new stress–strain model based on Haldane's distribution function (Haldane, 1919) which allows one to predict the stress–strain relationship over the whole pre-failure strain range using only one datum point (peak axial stress and maximum axial strain at this peak stress). The proposed model is suitable for weak to strong ($\sigma_c < 100$ MPa) carbonate rocks (chalk, dolomites and limestones) exhibiting axial strains up to 1%. It is shown that the stress–strain curves observed in laboratory compression tests at Ben-Gurion University (Beer-Sheva, Israel) are similar to those predicted by the proposed model. To the author's knowledge, so far no results of experimental work have been published, which describe the stress–strain relationship using Haldane's distribution function.

2. New Stress–Strain Model Based on Haldane's Distribution Function

Distribution functions have many interesting mathematical properties, and therefore they are widely used in science and engineering. Examples of their uses are: radioactive decay, capacitor charging and discharging, rates of chemical reactions, population growth, inflation in economics, engineering geology and many more. In particular,

engineering geology uses a Weibull distribution to estimate the earthquake occurrence (Hagiwara, 1973) and the failure probability of rocks under mechanical loading (Weibull, 1939; Kettl and Diaz, 1988; Lawn, 1993; Gupta and Bergstrom, 1998), a Gaussian (normal) distribution to predict the gob gas well productivity (Palchik, 2002) and the subsidence of undermined rock masses (Muller, 1958), and a Poisson's distribution to predict the development of Karst processes (Mulyukov, 1998), etc.

However, the use of the above-mentioned distribution functions to create a stress–strain model is not convenient, since it requires the determination of at least three unknown parameters and, hence, at least three data points are necessary. For example, consider a canonical form of the Weibull distribution (Weibull, 1939) which is widely used to estimate the failure probability of rock samples under mechanical loading:

$$W(x) = 1 - \frac{1}{e^{\left(\frac{x}{k}\right)^m}}, \tag{4}$$

where W(x) is the Weibull function, x is a variable parameter, k and m are unknown constants, e is Euler's number ($e = 2.718$).

Assuming that $W(x) = \sigma_a$ and $x = \varepsilon_a$, the Weibull function for possible prediction of the stress–strain relationship may have three unknown constants (k, m and λ):

$$\sigma_a = \lambda\left[1 - \frac{1}{e^{\left(\frac{\varepsilon_a}{k}\right)^m}}\right], \tag{5}$$

where σ_a is axial stress (in MPa), ε_a is axial strain (in %) at axial stress σ_a, λ is a parameter which reflects the influence of mechanical properties.

It is desirable to use only distribution functions which have a small number of unknown constants, and, naturally, mathematical forms which are suitable for a stress–

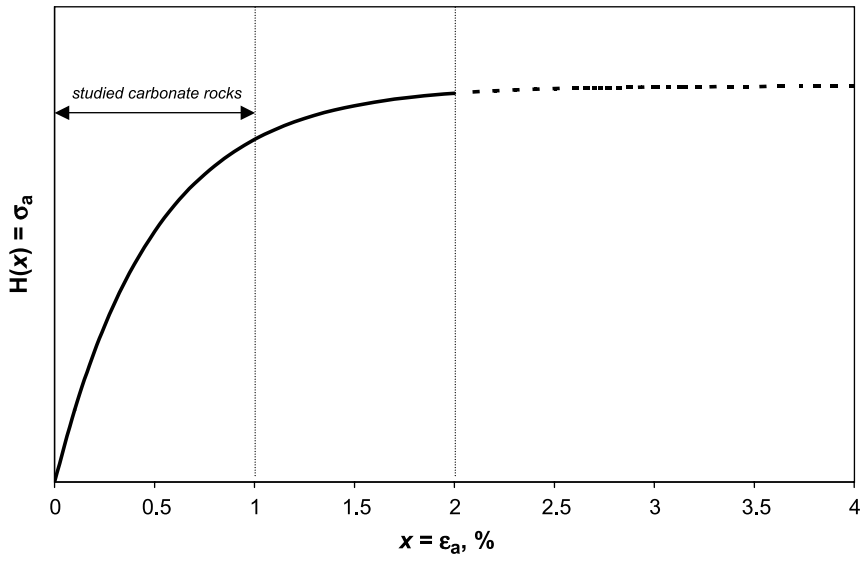

Fig. 2. Dependence of H(x) on x according to Haldane's function (Eq. (6)), ——— first segment, - - - second segment

strain model. Therefore, the author suggests using Haldane's distribution function (Haldane, 1919) that relates the probability (H(x)) of recombination between two loci to their map distance (x). This suggestion is made for the following reasons:

1) Haldane's distribution function has only known constants $\left(\frac{1}{2}\text{ and }2\right)$:

$$H(x) = \frac{1}{2}\left(1 - \frac{1}{e^{2x}}\right) \tag{6}$$

2) The curve $\mathrm{H}(x) - x$ (Eq. (6)) presented in Fig. 2 may be suitable for stress–strain descriptions when we assume that $\mathrm{H}(x) = \sigma_a$ and $x = \varepsilon_a$ since:

- $\mathrm{H}(x) = \sigma_a = 0$ when the parameter of $x = \varepsilon_a = 0$ (zero stress at zero strain).
- $\mathrm{H}(x) = \sigma_a$ is always positive at positive $x = \varepsilon_a$.

Table 1. Summary of test results

Rock	Sample	σ_c, MPa	$\varepsilon_{a\ max}$, %	E, MPa	n, %	λ
Adulam chalk	RC1	53.2	0.32	17400	21.5	224
	RC3	51	0.41	16000	23.3	190
	RC4	31.9	0.32	11700	28.5	138
	RC6	63.3	0.41	19250	20.7	230
	RC7	32.1	0.41	9500	30	116
	RC8	60.3	0.37	17300	21.9	224
	RC9	63.1	0.31	20500	19.6	266
	ST1A	50.9	0.37	16200	20.5	198
	ST1B	53.7	0.39	15400	20.2	202
	ST2A	52.25	0.4	14300	20.7	196
	ST2B	37.4	0.34	10700	23.7	152
Aminadav dolomite	AD5	97.8	0.2	56000	5.8	590
	AD15	67.2	0.25	29000	20.9	340
	AD83	61.6	0.34	18000	15.4	235
Beit-Meir dolomite	BM2	71.5	0.25	38100	17.1	370
	BM3	45.6	0.22	21400	29	245
Bina limestone	Bina 5	80	0.22	38700	13.6	424
	Bina 6	89	0.48	24800	10.4	300
	Bina 7	64	0.29	25000	14.3	284
	TH5-15	84	0.25	37700	13.6	430
	TH3-24	15.4	0.18	10000	21.8	100
	TH5-13	31.3	0.14	24000	21.4	264
	B1	66.5	0.19	43100	7.5	430
	B2	25	0.16	20900	21.1	190
	B3	35	0.19	21000	26.4	216
	B4	14	0.15	11500	37.9	114
	B5	98	0.29	35200	13.7	436
	B7	54.4	0.78	10900	20	140
Sorek dolomite	BZ5-16	78	0.4	24300	17.5	282
	BZ2-61A	85.8	0.5	22300	13.6	270
Yarka limestone	Yarka1	38.7	0.63	6500	15.7	108
	Yarka2	38.7	0.74	6200	17.9	99
	Yarka3	41	0.69	6200	17.9	108
	Yarka4	71	1.07	8400	16.4	158

Legend: σ_c is the uniaxial compressive strength, $\varepsilon_{a\ max}$ is maximum axial strain, E is elastic modulus, n is porosity, λ is the observed parameter for Eq. (7) using the method of successive approximations.

- $H(x) = \sigma_a$ increases from 0 to its maximum value with increasing $x = \varepsilon_a$ (in %) from 0 to 2% (first segment). When $x = \varepsilon_a > 2\%$ (second segment), no increase in $H(x) = \sigma_a$ occurs. Since the studied carbonate rocks exhibit $\varepsilon_a < 1\%$ (see Table 1), the left half of first segment of the curve $H(x) - x$ (see Fig. 2) may be suitable for stress–strain predictions of these rocks.
- The left half of the first segment of the curve $H(x) - x$ is linear at small axial strains ($x = \varepsilon_a$), while at relatively large axial strains it is slightly concave upward, which is typical of stress–strain relationship for the studied carbonate rocks.

Let us therefore assume that the inserting $\sigma_a = H(x)$ and $\varepsilon_a = x$ in Eq. (6) may give the possible stress–strain model to describe the stress (σ_a) – strain (ε_a) relationship from zero stress at zero strain up to failure:

$$\sigma_a = \frac{\lambda}{2}\left(1 - \frac{1}{e^{2\varepsilon_a}}\right). \tag{7}$$

Here, there is only one unknown parameter λ, which reflects the influence of mechanical properties.

Of course, the assumption that the above-mentioned mathematical expression (Eq. (7)) may be used to predict the stress–strain relationship requires detailed examination based on the comparison of the observed and predicted stress–strain relationships as discussed below in Section 4.

3. Testing

Stress–strain relationships for six different carbonate rocks (Adulam chalk, Aminadav dolomite, Beit-Meir dolomite, Bina limestone, Sorek dolomite and Yarka limestone) were observed at the Rock Mechanics Laboratory of the Ben-Gurion University. The chalk, dolomite and limestone samples were taken from different regions of Israel. Rock samples were prepared following ISRM suggested methods with NX size (diameter of 54 mm and length/diameter ratio of 2). The samples were ground to a planeness of 0.01 mm and cylinder perpendicularity within 0.05 radians.

The load frame used in this study (TerraTek system, model FX-S-33090) operates under hydraulic closed-loop servo-control with a maximum axial force of 1.4 MN and load frame stiffness of 5×10^9 N/m. The load was measured by a sensitive load cell located in series with the sample having a maximum capacity of 1000 kN and a linearity of 0.5% of full scale. The axial strain cantilever set has a 10% strain range, and the radial strain cantilevers have a strain range limit of 7%, with linearity of 1% for the full scale in both sets. The load frame and sample with radial and axial cantilever sets are described in detail elsewhere (Palchik and Hatzor, 2000; Palchik and Hatzor, 2004). All samples were tested at a constant strain rate of 10^{-5}/s and at an ambient temperature of 25°. The load frame is presented in Fig. 3a.

Mechanical properties of carbonate rocks from the Adulam, Aminadav, Beit-Meir, Bina, Sorek and Yarka formations are summarized in Table 1. Samples presented in Table 1 were selected to be free of cracks, fissures and veins, which would act as planes of weakness and have an undesirable effect on the stress–strain curves. Note that Table 1 includes only rock specimens which may be described according to the

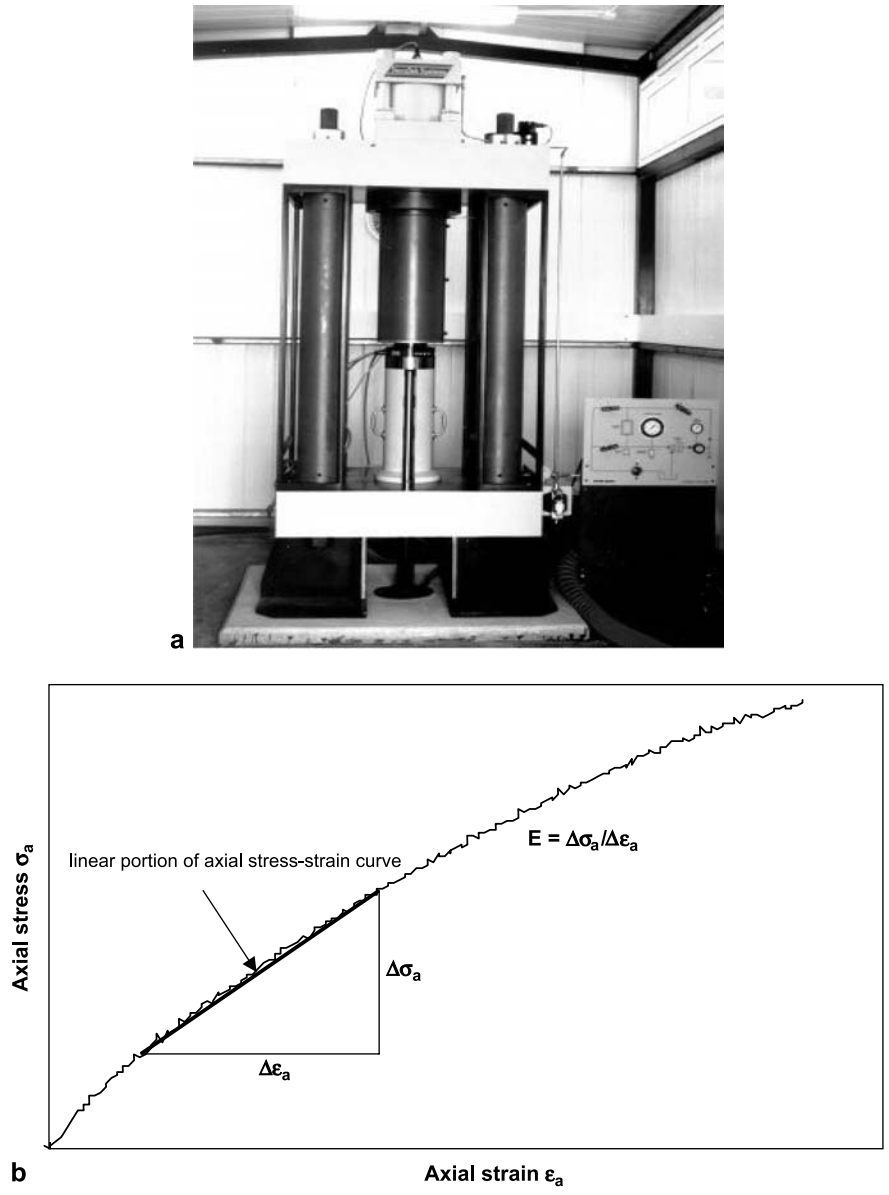

Fig. 3. Mechanical testing at the Rock Mechanics Laboratory of the Negev: **a**) load frame, **b**) determination of the elastic modulus

ISRM suggested methods (ISRM, 1981) as weak ($5 < \sigma_c < 25$ MPa), medium strong ($25 < \sigma_c < 50$ MPa) and strong ($50 < \sigma_c < 100$ MPa), where σ_c is the uniaxial compressive strength. Very strong and extremely strong samples ($\sigma_c > 100$ MPa according to the ISRM suggested methods) were omitted in this study. We did perform only few

unconfined compression tests on very strong and extremely strong carbonate samples that are insufficient for a detailed analysis. The development of the stress–strain model based on Haldane's distribution function for carbonate rock exhibiting $\sigma_c > 100$ MPa is subject to further investigation.

The values of the uniaxial compressive strength (σ_c) in Table 1 are between 14 and 98 MPa, maximum axial strain ($\varepsilon_{a\,max}$) at σ_c ranges between 0.14 and 1.07%, elastic modulus (E) values range from 6200 to 56000 MPa, and the porosity values (n) have a range of $5.8 < n < 37.9\%$. The elastic modulus (E) was determined as the slope of linear portion of the axial stress–strain curve (see Fig. 3b): $E = \Delta\sigma_a/\Delta\varepsilon_a$ where $\Delta\sigma_a$ and $\Delta\varepsilon_a$ are changes in axial stress and strain, respectively. Porosity (n) was calculated ($n = (1 - \rho/G_s) \times 100\%$) from measured values of dry bulk density ($\rho = 1.68$–$2.54\,g/cm^3$) and specific gravity of the solids ($G_s = 2.7\,g/cm^3$). The precision of the porosity estimation is 0.1%.

Physical properties of the studied rock formations and their microstructural characteristics are presented in detail elsewhere (Hatzor and Palchik, 1997, 1998; Palchik and Hatzor, 2002, 2004).

4. Examination of Proposed Stress–Strain Model

The assumed stress–strain prediction model (7) based on Haldane's distribution function is valid only when:

- It is evident that there are values of the parameter λ at which the predicted and observed (at laboratory testing) stress–strain relationships are similar.
- The parameter λ has a physical meaning.
- Values of the parameter λ are pre-known.

4.1 Statistical Determination of Values of the Parameter λ

Inserting initially assumed values of $\lambda = 20, 30, \ldots, 100$, and then $200, 300, \ldots, 1000$ into the model (7) and using a statistical method of successive approximations, we have determined that there are values of the parameter λ (between 99 and 590) at which the observed stress–strain curve in each of the studied rock samples can be described by Eq. (7). In order to explain in detail the statistical technique, consider, for example, determination of λ for sample RC9 (Fig. 4). Let us assume that $\lambda = 50$. Figure 4 shows that the calculated stress–strain curve (Eq. (7), $\lambda = 50$) is located below the observed stress–strain curve. This fact suggests that the value of $\lambda = 50$ is too small and, therefore, it must be increased. We then assume that the value of $\lambda = 100$. However, in this case, calculated stress–strain curve (Eq. (7), $\lambda = 100$) is still below the observed stress–strain curve. This means that the value of λ must be increased again. We then assume that the value of $\lambda = 300$ and see from Fig. 4 that the calculated stress–strain curve (Eq. (7), $\lambda = 300$) is located above the observed stress–strain curve. This means that the value of λ is too large and, therefore, that it must be decreased. We again change the value of λ using successive approximations and, finally, determine that $\lambda = 266$ since, in this case, observed and calculated (with $\lambda = 266$) stress–strain relationships are similar.

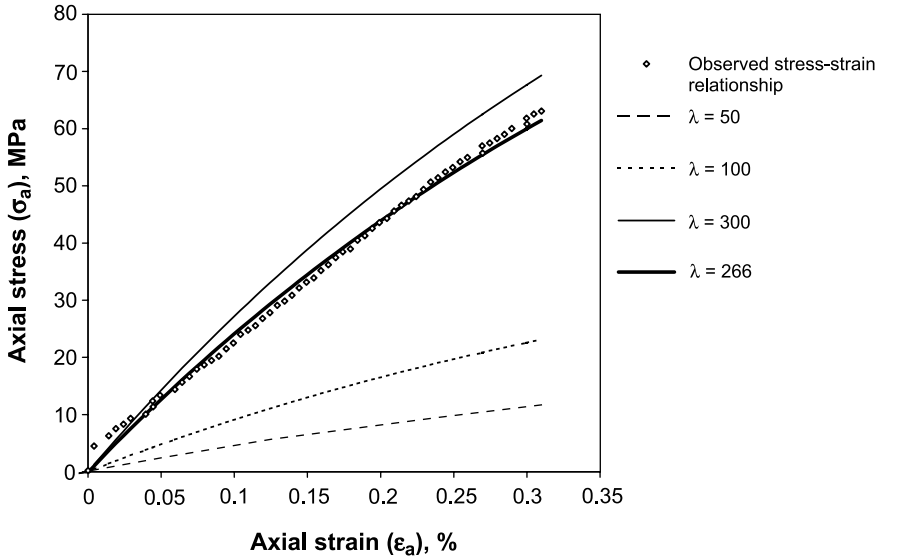

Fig. 4. Example of determination of λ (sample RC9) using the method of successive approximations

Figures 5–10 show examples of the observed and predicted (Eq. (7)) stress–strain curves for four Adulam chalk samples ($\lambda = 116$, 152, 224 and 266), two Aminadav dolomite samples ($\lambda = 235$ and 590), two Beit-Meir dolomite samples ($\lambda = 245$ and 370), four Bina limestone samples ($\lambda = 100$, 264, 300 and 436), two Sorek dolomite samples ($\lambda = 270$ and 282) and two Yarka dolomite samples ($\lambda = 108$ and 158),

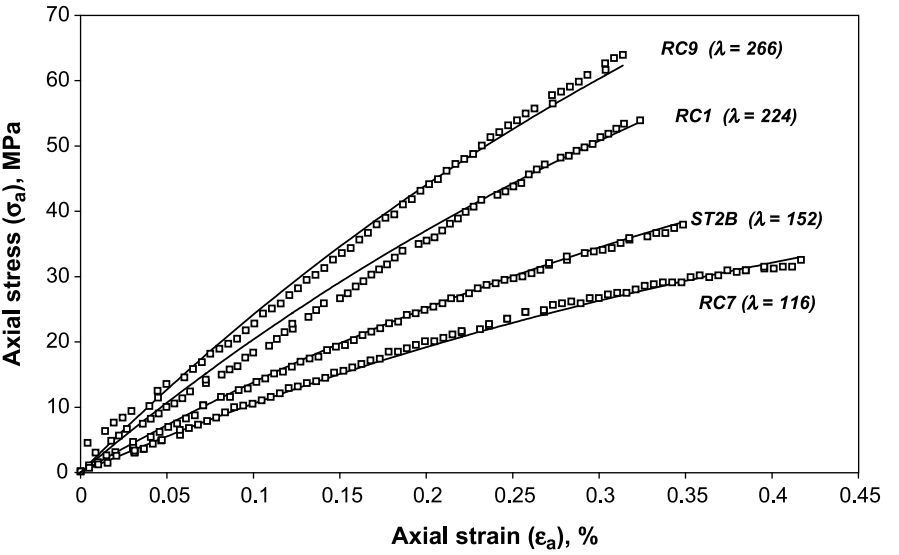

Fig. 5. Observed (□) and predicted (——) (Eq. (7)) stress–strain relationships for different samples of Adulam chalk

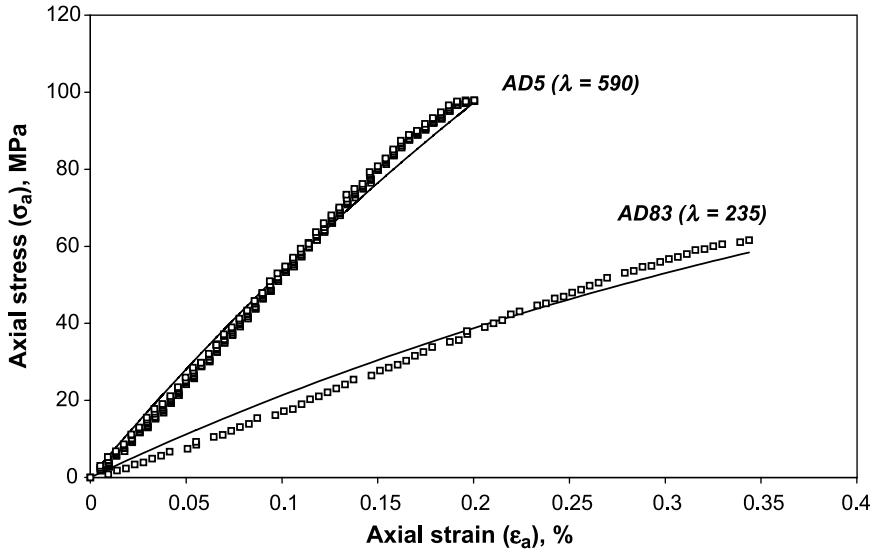

Fig. 6. Observed (□) and predicted (——) (Eq. (7)) stress–strain relationships for different samples of Aminadav dolomite

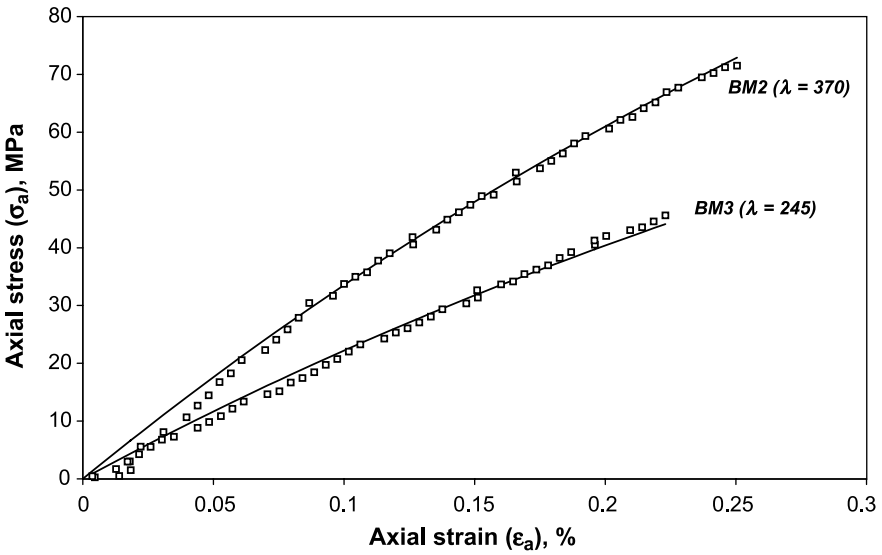

Fig. 7. Observed (□) and predicted (——) (Eq. (7)) stress–strain relationships for different samples of Beit-Meir dolomite

respectively. The values of λ (in brackets) in Figs. 5–10 were obtained using the method of successive approximations.

Values of the parameter λ observed in each of the studied samples using the method of successive approximations are also reported in Table 1. It should be noted

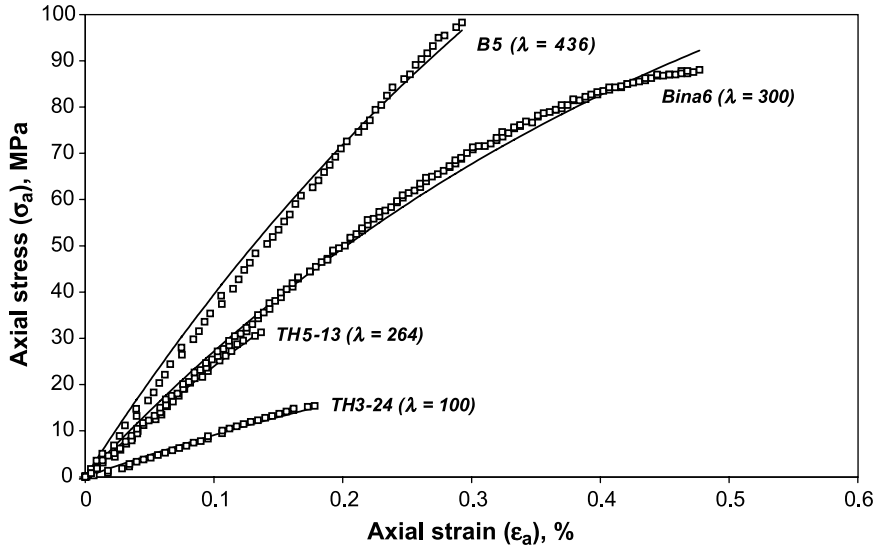

Fig. 8. Observed (□) and predicted (——) (Eq. (7)) stress–strain relationships for different samples of Bina limestone

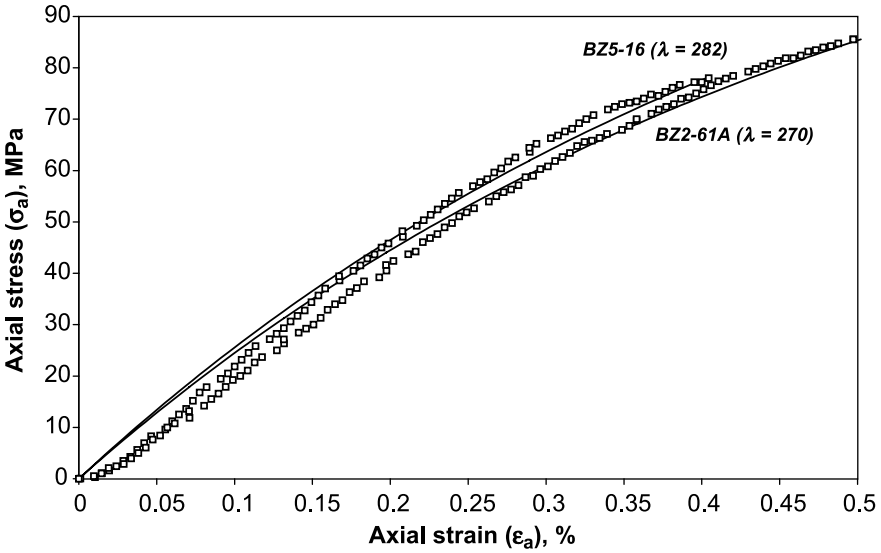

Fig. 9. Observed (□) and predicted (——) (Eq. (7)) stress–strain relationships for different samples of Sorek dolomite

that the parameter λ is not constant even for a single set of samples within the same rock: $116 < \lambda < 266, 235 < \lambda < 590, 245 < \lambda < 370, 100 < \lambda < 436, 270 < \lambda < 282$ and $99 < \lambda < 158$ for Adulam chalk, Aminadav dolomite, Beit-Meir dolomite, Bina limestone, Sorek dolomite and Yarka dolomite, respectively. The explanation of this scatter in the values of λ is presented in the next section.

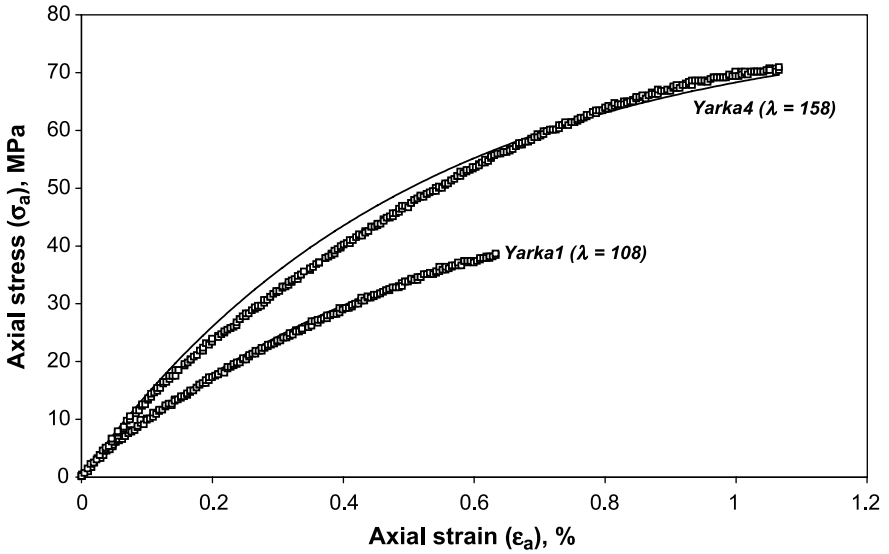

Fig. 10. Observed (□) and predicted (——) (Eq. (7)) stress–strain relationships for different samples of Yarka limestone

4.2 Physical Meaning of the Parameter λ

In order to determine the physical meaning of the parameter λ, the latter was plotted versus elastic modulus (E), porosity (n) and uniaxial compressive strength (σ_c) in each of the studied samples (see Fig. 11). Here thin, thick continuous and dashed lines show

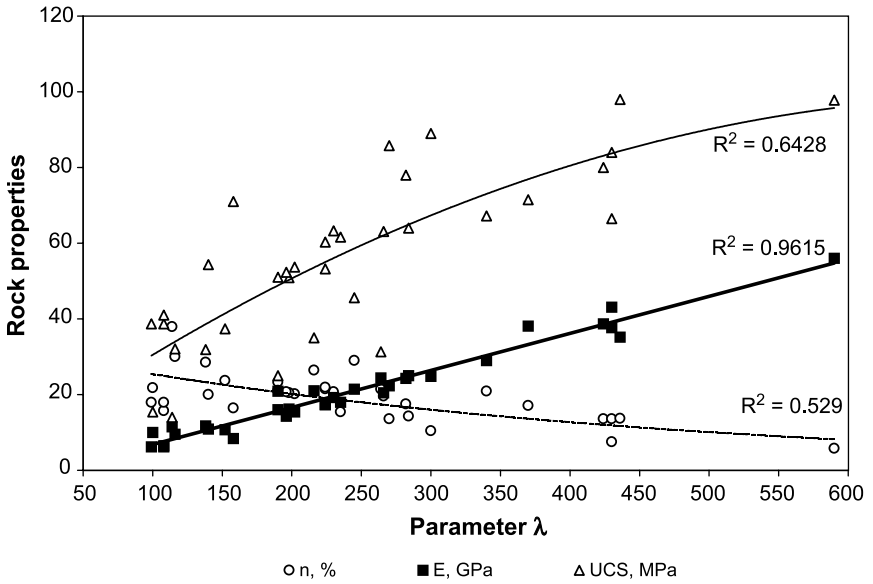

Fig. 11. Observed parameter λ versus elastic modulus (E, GPa), porosity (n, %) and uniaxial compressive strength (σ_c, MPa) for all studied samples. Thin, thick continuous and dashed lines show the best fit for $\sigma_c - \lambda$, $E - \lambda$ and $n - \lambda$ dependencies, respectively

the best fit for $\sigma_c - \lambda$, $E - \lambda$ and $n - \lambda$ dependencies, respectively. Figure 11 allows one to make the following observations:

- Porosity (n) and uniaxial compressive strength (σ_c) are only weakly correlated with the parameter λ ($R^2 = 0.529$ and 0.6428, respectively).
- On the other hand, the parameter λ seems to correlate well ($R^2 = 0.9615$) with elastic modulus (E).

The relationship between the parameter λ and elastic modulus (E) can be approximated by the following linear expression:

$$\lambda = aE + b, \tag{8}$$

where E is expressed in MPa, a and b are empirical coefficients: $a = 0.098$, $b = 38.18$.

Note, however, that the relative error (Δ) between the statistically observed (Table 1) and calculated (Eq. (8)) parameter λ can be as high as 27–31%. Figure 12 shows the relative errors between calculated (Eq. (8)) and observed λ in each of the studied samples, which are represented by closed circles. The x-axis shows the observed λ for each of studied samples. The relative error (Δ) between the observed and calculated λ has been calculated as

$$\Delta = \frac{|\lambda_{obs} - \lambda_{cal}|}{0.5(\lambda_{obs} + \lambda_{cal})} 100\%, \tag{9}$$

where λ_{obs} and λ_{cal} are the observed and calculated values of the parameter λ, respectively.

Thus, the expression (8) is only used to show the physical meaning of the parameter λ and is not to be considered to be precise. Since the parameter λ is related to

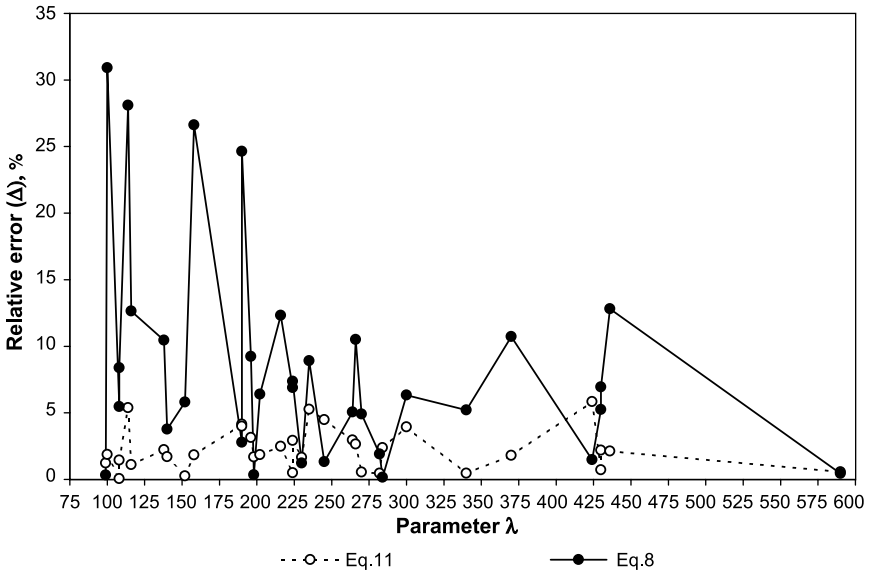

Fig. 12. Relative errors between calculated (Eqs. (8) and (11)) and observed λ for each of studied samples. The closed and open circles represent the relative errors for Eqs. (8) and (11), respectively

stiffness (elastic modulus) of the rock samples, a large scatter in parameter λ is probably due to a large scatter in elastic modulus of the different rock samples: an increase in the elastic modulus by a factor of 9 (from 6.2 to 56 GPa) leads to an increase in λ by a factor of 6 (from 99 to 590) as shown in Fig. 11.

5. Discussion

It is clear that the stress–strain prediction requires the prior knowledge of the parameter λ that cannot be precisely obtained from Eq. (8) as discussed above. However, the value of λ can be obtained from the model (7) when there is only one point measurement (i.e., axial stress and axial strain in the same point):

$$\lambda = \frac{2\sigma_{a1}}{1 - \frac{1}{e^{2\varepsilon_{a1}}}}, \tag{10}$$

where σ_{a1} and ε_{a1} are axial stress and axial strain measured at the same point.

When we know the stress and strain at the final point of pre-failure strain (i.e. when $\sigma_{a1} = \sigma_c$ and $\varepsilon_{a1} = \varepsilon_{a\,max}$) the model (10) can be rewritten as:

$$\lambda = \frac{2\sigma_c}{1 - \frac{1}{e^{2\varepsilon_{a\,max}}}}. \tag{11}$$

The relative error (Δ, Eq. (9)) between the calculated (Eq. (11)) and statistically observed (see Table 1) parameter λ is relatively small ($0.045 < \Delta < 5.84\%$), as shown in Fig. 12. In Fig. 12 these relative errors between the calculated and observed λ for each of the studied samples are represented as open circles.

Figure 13 shows a comparison between the observed and calculated (Eq. (8) and Eq. (11)) parameter λ. Although, Eq. (8) has a relatively good squared regression coefficient ($R^2 = 0.9615$, Fig. 13a), the value of 0.9615 is insufficient to decrease the relative errors between calculated (Eq. (8)) and observed parameter λ in Fig. 12. Only the use of Eq. (11) (with very good $R^2 = 0.996$, Fig. 13b) allows one to decrease these errors (see Fig. 12). Figure 13c demonstrates the relatively large vertical distances (errors) between values of λ calculated according to Eq. (8) and the linear slope of $s = 1$, whereas such errors for λ calculated according to Eq. (11) is small. The large errors presented in Fig. 13c correspond to maximum relative errors in Fig. 12.

Inserting Eq. (11) into Eq. (7) provides the final model based on Haldane's distribution function for predicting the stress–strain relationship:

$$\sigma_a = \frac{\sigma_c}{A}\left[1 - \frac{1}{(e^{\varepsilon_a})^2}\right], \tag{12}$$

where $A = 1 - (1/e^{2\varepsilon_{a\,max}})$, σ_c is the uniaxial compressive strength and $\varepsilon_{a\,max}$ is the maximum axial strain.

Fig. 13. Comparison between observed and calculated (Eqs. (8) and (11)) values of λ: **a**) calculated (Eq. (8)) versus observed λ, **b**) calculated (Eq. (11)) versus observed λ, **c**) calculated (Eqs. (8) and (11)) versus observed λ (the closed ● and open circles ○ represent the λ calculated according to Eqs. (8) and (11), respectively)

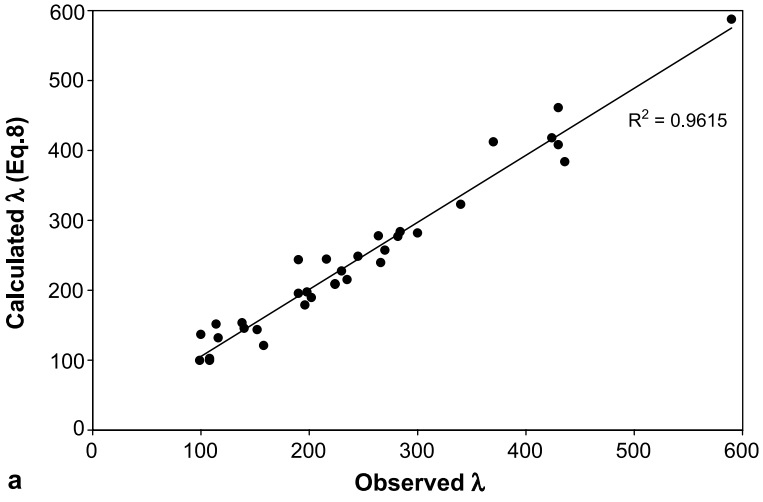
Calculated λ (Eq.8)
Observed λ
R^2 = 0.9615
0
100
200
300
400
500
600

a

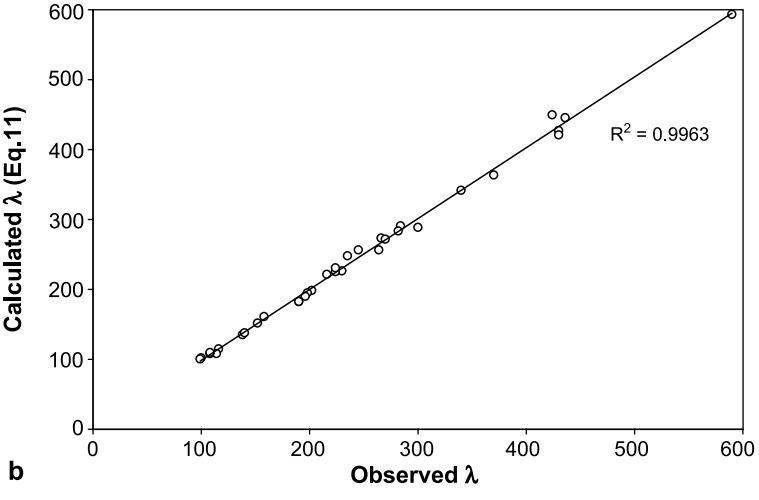
Calculated λ (Eq.11)
Observed λ
R^2 = 0.9963
0
100
200
300
400
500
600

b

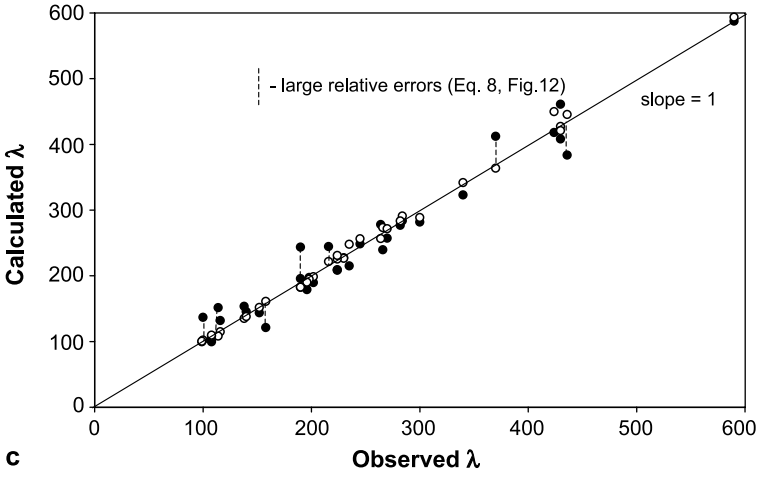
Calculated λ
Observed λ
large relative errors (Eq. 8, Fig.12)
slope = 1
0
100
200
300
400
500
600

c

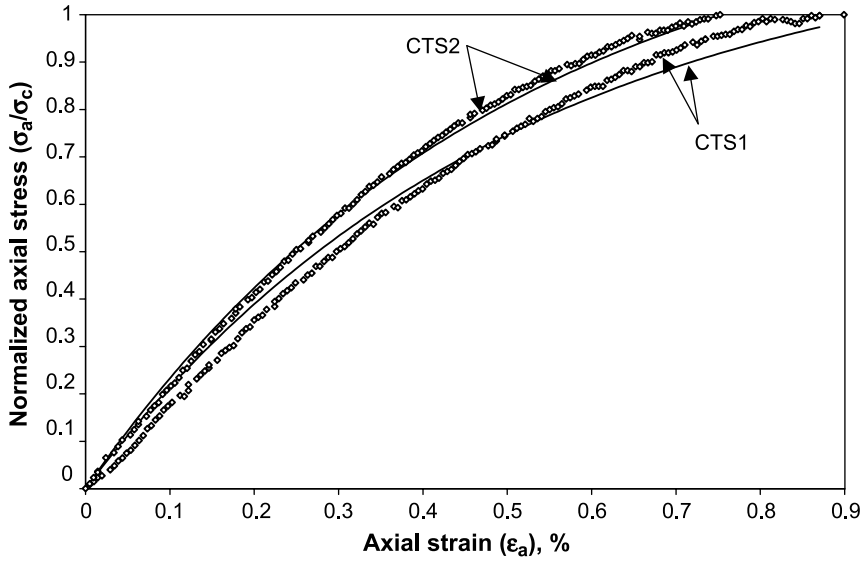

Fig. 14. Examination of model (12) for Tel-Sheva chalk which was not involved in determination of parameter λ; ◇ observed and —— calculated normalized axial stress

The final model (12) relates the axial stress (σ_a) to the square of an exponential function where the exponent is axial strain (ε_a). The proposed model (12) can be used to predict the stress–strain relationship over the whole pre-failure strain range for weak to strong carbonate rocks (σ_c <100 MPa) when the uniaxial compressive strength (σ_c) and maximum axial strain ($\varepsilon_{a\,max}$) at σ_c are known.

To show the validity of the proposed relation we used two Tel-Sheva chalk samples which were not involved in determination of parameter λ. These samples (CTS1 and CTS2) exhibit uniaxial compressive strengths of $\sigma_c = 24.5$ and 23.2 MPa, respectively, and maximum axial strains of $\varepsilon_{a\,max} = 0.94$ and 0.75%, respectively. Inserting values of σ_c and $\varepsilon_{a\,max}$ in the model (12) allows one to calculate the normalized axial stress (σ_a/σ_c) over entire pre-failure strain range for samples CTS1 and CTS2. The comparison of the calculated (Eq. (12)) and observed normalized axial stresses for these two samples is presented in Fig. 14, which shows that the observed and predicted σ_a/σ_c are similar. Thus, model (12) is also suitable for Tel-Sheva chalk.

6. Conclusions

A stress–strain prediction model based on Haldane's distribution function for weak to strong carbonate rocks (σ_c <100 MPa) exhibiting axial strains less than 1% is proposed. The proposed analytical model relates the axial stress (or normalized axial stress) to the square of an exponential function of axial strain (ε_a). The comparison of the predicted and observed stress–strain curves shows that these curves are very close to each other and thereby confirms the suitability of Haldane's distribution function to predict the stress–strain relationships in carbonate rocks.

Only one datum point (peak stress and maximum axial strain at this peak stress) is needed to predict the stress–strain relationship over the entire pre-failure strain range in carbonate rocks using the proposed stress–strain prediction model.

References

Chang, C. S., Wang, T. K., van Meir, J. G. M. (2002): Fracture modeling using a micro-structural mechanics approach-I. Theory and formulation. Eng. Fract. Mech. 69, 1941–1958.

Ching, L. L., Ta, P. C., Dong, H. Y., Ching, S. C. (1997): Stress–strain relationship for granular materials based on hypothesis of best fit. Int. J. Solids Struct. 34(31–32), 4087–4100.

Duncan, J. M., Chang, C. Y. (1970): Non-linear analysis of stress and strain in soils. J. Soil Mech. Found. Div. Proc. Am. Soc. Civil Eng. 96 (SM5), 1629–1653.

Fairhurst, C. E., Hudson, J. A. (1999): Draft IRSM suggested method for the complete stress–strain curve for intact rock in uniaxial compression. Int. J. Rock Mech. Min. Sci. 36(3), 281–289.

Gupta, V., Bergstrom, J. S. (1998): Compressive failure of rocks by shear faulting. J. Geophys. Res. 103, 23875–23895.

Gutierrez, M., Kolderup, U. M., Hoeg, K. (2000): Model for 3D time-dependent chalk stress–strain behavior. Proc., 6th North Sea Symp., Brington, UK.

Haas, C. J. (1989): Static stress–strain relationships. In: Touloukian, Y. S., Judd, W. R., Roy R. F. (eds), Physical properties of rocks and, minerals. 2. Hemisphere Publishing, Taylor and Francis, London, 123–176.

Habimana, J., Labiouse, V., Decoeudres, F. (2002): Geomechanical characterisation of cataclastic rocks: Experience from the Cleuson-Dixence project. Int. J. Rock Mech. Min. Sci. 39(6), 677–693.

Hagiwara, Y. (1973): An application of Weibull distribution function to probability of earthquake occurrence. J. Geodet. Soc. Japan 19(3), 171–173.

Haldane, J. B. S. (1919): The combination of linkage values and the calculation of distances between the loci of linked factors. J. Genetics 8, 299–309.

Hatzor, Y. H., Palchik, V. (1997): The influence of grain size and porosity on crack initiation stress and critical flaw length in dolomites. Int. J. Rock Mech. Min. Sci. 34(5), 805–816.

Hatzor, Y. H., Palchik, V. (1998): A microstructure-based failure criterion for Aminadav dolomites. Int. J. Rock Mech. Min. Sci. 35(6), 797–805.

ISRM (1981): Brown, E. T. (ed.). Suggested methods for rock characterization, testing and monitoring. Pergamon Press, Oxford.

Kettl, P., Diaz, G. (1988): Weibull's fracture statistics or probalistic strength of materials: State of art. Res Mech 24, 99–207.

Kodner, R. B. (1963): Hyperbolic stress–strain response: cohesive soils. Jour. of the Soil Mechanics and Foundation Division. Proc., Am. Soc. Civil Eng. 89, (SM1), 115–143.

Lawn, B. (1993): Fractures of brittle solids, 2nd edn. Cambridge University Press, Cambridge.

Muller, P. A. (1958): Influence of mining workings on movement of ground surface. Moscow, Ugletexizdat.

Mulyukov, E. I. (1998): The karst process and construction on lands prone to karst formation (in Bashkorstostan as an example). Soil Mech. Found. Eng. 35(1), 17–21.

Muravskii, G. B. (1996): On analytical description of stress–strain relationship for rocks and soils. Commun. Numer. Methods Engng. 12(12), 827–834.

Palchik, V., Hatzor, Y. H. (2000): Correlation between mechanical strength and microstructural parameters of dolomites and limestones in the Judea group – Israel. Isr. J. Earth Sci. 49(2), 65–79.

Palchik, V., Hatzor, Y. H. (2002): Crack damage stress as a composite function of porosity and elastic matrix stiffness in dolomites and limestones. Eng. Geol. 63(3–4), 233–245.

Palchik, V. (2002): Use of Gaussian distribution for estimation of gob gas drainage well productivity. Mathemat. Geol. 34(6), 743–765.

Palchik, V., Hatzor, Y. H. (2004): The influence of porosity on tensile and compressive strength of porous chalks. Rock Mech. Rock Engng. 37(4), 331–341.

Puzrin, A. M., Burland, J. B. (1996): A logarithmic stress–strain function for rocks and soils. Geotechnique 46(1), 157–164.

Shibuya, S. (2002): A non-linear stress-stiffness model for geomaterials at small to intermediate strains. Geotechn. Geol. Engng. 20(4), 333–369.

Tatsuoka, F., Shibuya, S. (1992): Deformation characteristics of soils and rocks from field and laboratory tests. Proc., 9th Asian Conf. Soil Mech. and Foundation Engineering. Bangkok 2, 101–170.

Tharp, T. M., Scarbrough, M. G. (1994): Application of hyperbolic stress–strain models for sandstone and shale to fold wavelength in Mexican Ridges Foldbelt. J. Struct. Geol. 16(12), 1603–1618.

Weibull, W. (1939): A statistical theory of the strength of materials. Ing. Vetenskaps Akad. Handl. 151, 1–45.

Author's address: Dr. V. Palchik, Department of Geological and Environmental Sciences, Ben-Gurion University of the Negev, P.O. Box. 653, Beer-Sheva, 84105, Israel; e-mail: vplachek@bgumail.bgu.ac.il